STAG: Smart Tools and Applications in Graphics (2018)
M. Livesu, G. Pintore and A. Signoroni (Editors)

Hyperquadrics for shape analysis of 3D nanoscale reconstructions of brain cell nuclear envelopes

M. Agus [1,3], C. Calì [2], A. Tapia Morales [1], H. O. Lehväslaiho [4], P. J. Magistretti [2], E. Gobbetti [3] and M. Hadwiger [1]

[1] King Abdullah University of Science and Technology (KAUST)
Visual Computing Center (VCC), Thuwal 23955-6900, Saudi Arabia
[2] King Abdullah University of Science and Technology (KAUST)
Biological and Environmental Science and Engineering (BESE), Thuwal 23955-6900, Saudi Arabia
[3] Center for Advanced Studies, Research and Development in Sardinia (CRS4)
Visual Computing Group, Cagliari, Italy
[4] CSC - IT Center for Science, Espoo, Finland

Abstract

Shape analysis of cell nuclei is becoming increasingly important in biology and medicine. Recent results have identified that the significant variability in shape and size of nuclei has an important impact on many biological processes. Current analysis techniques involve automatic methods for detection and segmentation of histology and microscopy images, and are mostly performed in 2D. Methods for 3D shape analysis, made possible by emerging acquisition methods capable to provide nanometric-scale 3D reconstructions, are, however, still at an early stage, and often assume a simple spherical shape. We introduce here a framework for analyzing 3D nanoscale reconstructions of nuclei of brain cells (mostly neurons), obtained by semiautomatic segmentation of electron micrographs. Our method considers an implicit parametric representation customizing the hyperquadrics formulation of convex shapes. Point clouds of nuclear envelopes, extracted from image data, are fitted to our parametrized model, which is then used for performing statistical analysis and shape comparisons. We report on the preliminary analysis of a collection of 92 nuclei of brain cells obtained from a sample of the somatosensory cortex of a juvenile rat.

1. Introduction

In biology, the nucleus is a membrane-enclosed organelle found in eukaryotic cells, including the ones composing the brain. It represents the control center of the cell, since, in particular, it organizes activities by regulating gene expression. The nuclear envelope separates the cell nucleus and cytoplasm. It consists of an inner and outer membrane, separated by peri-nuclear space and perforated by nuclear pores. All active and passive transport processes in and out of the nucleus take place via the nuclear pores.

Geometrically, the cell nucleus has been often studied as a spherical structure [FHWV97]. This approximation is increasingly proving way too coarse for a number of applications. Recently, the analysis of proteins associated with the nuclear envelope in rat hippocampal neurons provided evidence that the geometry of nuclei is far more complex [QWBW08], and that the shape of cell nuclei is likely to influence the nucleo-cytoplasmic exchange of macromolecules and ions, in particular calcium, which is a key regulator of neuronal gene expression. Moreover, the size and shape of nuclear envelopes can vary not only among species, abut also within species and even within single individuals, depending on cell types and other, even transient, conditions. The analysis of shape properties is thus gaining importance in biology and medicine, since shape variability can provide indicators of different conditions and can provide hints for classifying cells.

A major field in which cell nucleus analysis is considered of paramount importance is computer aided diagnostics [XY16], where a series of methods have been developed for automated 2D detection and segmentation on microscopy images, with the aim of providing support for various quantitative analyses, including calculating cellular morphology, including size, shape, or texture. However, most of nuclear analysis is performed directly on 2D images, and only few efforts have used 3D reconstruction, in particular for studying the dynamics of nuclear infoldings in response to neuronal activity [WQE*09]. It is only very recently, with the emergence of digital acquisition methods capable to provide 3D reconstructions at nanometric resolution scale [CBB*16], that collections of 3D shape measurements of nuclei are starting to become available. Hence, the need is arising to develop shape analysis frameworks to support domain scientists in performing 3D quantitative measures, classification and clustering operations, e.g., for associating different shapes to different nuclear conditions.

In this paper, we consider digital 3D reconstructions of nuclei of

DOI: 10.2312/stag.20181304

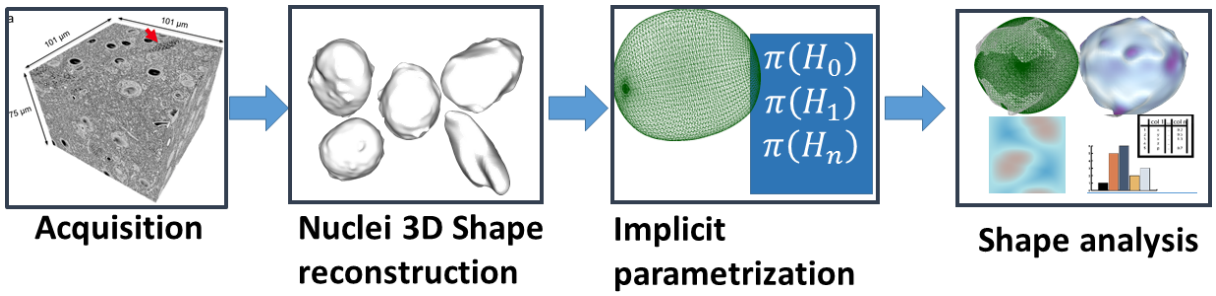

Figure 1: ***Method overview:*** *from 3D nanoscale reconstructions of neuron nuclei obtained from electron microscopy image stacks, we fit specific implicit surface representations in a way to derive parameter sets that can be used for shape analysis and classification.*

brain cells (mostly neurons), obtained by segmenting serial electron micrographs at nanoscale resolution, and we propose a shape analysis framework based on an implicit surface parametrization, which provides a simple but effective representation of nuclear envelope shapes. The obtained parameters can be used for providing measures, features, and indicators for shape classification. To this end, we adapted the *hyperquadrics* [Han88] implicit representation of convex shapes (see Fig. 1) using a formulation that provides us increased control in fitting the discrete point clouds representing the nuclei shapes as identified by image segmentation (see Sec. 4). We show how the fitting can be computed using a constrained optimization method (Sec. 4). From this implicit representation we then create an explicit radial representation by sampling (Sec. 5), which can be used for tessellation and shape comparison.

Our method makes it possible to obtain a parametric representation of shapes that can be used for measuring sizes, performing comparisons and for classifying nuclei with respect to different cells and conditions. Here, we demonstrate the method on a collection of 92 nuclear envelops of brain cells. The input data came from semiautomatic segmentation of electron micrographs of a sample of somatosensory cortex of a juvenile rat. We provide preliminary results of fitting performance of the proposed parametric model, as well as a discussion of a preliminary shape analysis performed by domain scientists with our framework.

The proposed framework is built around a specific implicit representation, hyperquadrics, that was chosen after visual assessment of neural nuclei envelopes according to domain scientists indications. The proposed model is shown to have increased sensitivity than the usual spherical approximation. It is accurate for convex neuron nuclei, but its accuracy suffers on concave and other contorted shapes. However, the described methodology can be considered general, and can be easily adapted to other parametric representations, based on implicit surface representations or function basis [SFM09], which can be able to describe more accurately general shapes presenting concavities.

2. Related work

The proposed method consists of creating a 3D shape analysis framework based on an implicit surface parametrization to be used for the study of 3D shapes obtained from nanoscale cell nuclear envelopes reconstructions. We discuss here the state-of-the-art in nuclei detection, shape analysis in neuroscience, and implicit representations in visual computing, by limiting our analysis to the methods that mostly relate to our techniques.

Cell nuclei segmentation. Accurate detection of individual cell nuclei in microscopy images is an essential and fundamental task for many biological studies. A comprehensive review of cell detection and segmentation algorithms can be found in [XY16]. The accuracy of segmentation and reconstructions determines the quality of morphology features extracted and is in some cases crucial for identifying and grading diseases. Broadly, three popular strategies are used for nucleus/cell segmentation: (a) separate the foreground from the background, and split the object groups into individual nuclei or cells [QXFY12, WHS*12]; (b) identify markers of nuclei or cells, and then, expand the markers to the object boundaries [VVDK*13, JKCO10, VVLVDDH13]; (c) generate a sufficient number of region candidates, and then, select the best ones as final segmentation [AM12, AK13, KVRR12]. Very recently, Ram et al. [RR16] presented a cell nucleus detection system using the fast radial symmetry transform (FRST), to be used in fluorescence in-situ hybridization (FISH) images obtained via confocal microscopy. To the best of our knowledge, all models are applied to 2D segmentation of cell nuclei. Our method fits parametric representations to 3D reconstructions of cell nuclear envelopes. It considers an extension of a generic implicit surface model that proves to be a simple but effective 3D parametric representation, expressive enough to perform statistical analysis and shape comparisons of rodent brain nuclear shapes.

Implicit representations in visual computing. A parametric representation of shape allows for the definition of geometrical objects using a few parameters and incorporating prior knowledge. Because implicit surfaces can be designed so that the algebraic distance to them can be quickly computed by evaluating a simple differentiable function, they are better suited to fitting 2D and 3D data that the most common explicit models [DG95]. One of the most common implicit representation is the superquadric, introduced by Barr in 1888 [Bar81] and, then widely applied to many problems, such as object representation [Pen86], shape recovery [SB90], image segmentation [GB93] and object modeling [TM90]. Superquadrics are, however, constrained to represent symmetrical-section volumes. This limitation was removed by Hanson [Han88] with the introduction of the hyperquadric primi-

tives, which include quadrics and superquadrics as special cases. Hyperquadrics are not symmetric and support taperings and distortions that are not naturally present within the conventional superquadric framework. The application of hyperquadrics can be mainly found in shape recovery [HGB93], but also in fitting models to sparse data [CC96]. Their 2D versions were used for 2D segmentation of nuclei shapes in nuclei observed with an epi-fluorescence microscope [CP00]. In this paper, we customize the hyperquadrics formulation for building a 3D shape analysis framework targeted to 3D nanoscale representations of brain cell nuclear shapes.

Shape analysis in neuroscience. The availability of 3D reconstructions of brain structures is driving the development of various frameworks for shape analysis in order to classify and account for variability to be associated to different structures and conditions. For a recent overview of the main methods employed in general for the analysis of brain structures, we refer reader to [NTDS14]. In general, shape analysis methods are mainly targeted to the full cortex acquired with MRI methods [WGK*15]. Recently, a study for 3D morphological analysis of asymmetric neuronal morphogenesis in developing zebrafish has been proposed [HJLC18], but in general shape analysis studies of brain structures at nanometric resolution are still lacking [CBB*16]. In the context of the specific analysis of nuclear envelopes, Queisser et al. [QWBW08] developed a tool to retrieve the 3-D view of cell nuclei from laser scanning confocal microscopy data. Their method extract surface information of the membrane by creating an isosurface with a marching tetrahedra algorithm combined with a modified Dijkstra graph-search algorithm, and it have been used to show how synaptic activity induces dramatic changes in the geometry of the cell nucleus [WQE*09]. Recent methods on 3D morphometric analysis consider frequency decomposition frameworks [SFM09], or functional spaces like Wesserstein space [SZW16], or Random Markov Fields [XBC18], and they are mostly used for studying hippocampi shapes [XBC18] or full cortex affected by Alzheimer disease [SZW16]. Here we focus on 3D reconstructions of brain cell nuclei, and, as far as we know, our method is the first attempt of 3D shape analysis based on implicit parametrization.

3. Method overview

The full pipeline of the proposed shape analysis framework is schematized in Fig. 3.

Data acquisition. The general workflow for 3D reconstruction and visual analysis of brain structures begins with sample preparation and 3DEM [KMWL08] imaging. Acquisition of biological tissues can be performed automatically at a z-resolution of 5-50 nanometers depending on the cutting technique [KMWL08]. After imaging, image stack needs preprocessing prior 3D reconstruction of the various cellular structures. First, the image stack needs to be aligned with the Stackreg tool available for ImageJ [TRU98]. Following image registration, the stack is then segmented, by means of manual or semi-automatic segmentation techniques [KVRKB*15]. Automated and semi-automated segmentation techniques reduce tremendously the time and effort needed to generate a first-pass three-dimensional model. In any case, this model then needs to be painstakingly proofread and corrected manually to achieve best results. The dataset so obtained includes high-resolution, segmented image stacks that can be visualized, explored and analyzed with a variety of tools based on either volume data representation, or surface mesh generated from the segmentations. Currently many neuroscientists take advantage of commercial or free software solutions [CSS*12, SSKH11] for 3D segmentation and reconstruction. In our case, we employ a semiautomatic method [HBK*16], and we perform surface reconstruction of the various nuclear envelopes with marching tetrahedra [TPG99]. For each nucleus, the vertices of the obtained 3D closed triangulated surfaces are used as input data for shape analysis.

Problem statement. Given a 3D point cloud representing a closed shape of a cell nucleus, we can define our fitting/analysis problem as finding the parameters of a surface model which better approximates the point cloud. Given a 3D surface, a surface representation can be defined implicitly as the function $H(x,y,x)$ such that the points of the surface respect the equation $H(x,y,z) = 1$. In this work, starting from qualitative assessment of nuclear shapes performed by domain scientists, we came out with the hypothesis that implicit *Hyperquadrics* [Han88] could provide effective representations of nuclear envelopes. Hence, we decided to develop our fitting/analysis framework around that model. In general, the fitting/analysis method is composed of three tasks:

- define and compute the parameters of the implicit representation;
- evaluate fitting by tessellating the fitting surface through computing an explicit representation;
- use the extracted parameters for statistical computations and analysis, and as predictive model for classifying different cell nuclei at varying conditions.

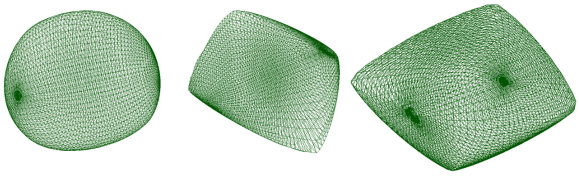

Figure 2: ***Hyperquadrics examples:*** *at varying of parameters of equation (1), various surfaces can be represented.*

Hyperquadrics representation. Hyperquadrics are implicit models defined by a sum of an arbitrary number of linear terms raised to powers, generating shapes whose bounding polytopes have an arbitrary number of faces [OS01]. A hyperquadric model is thus defined by the set of points satisfying:

$$H(x,y,z) = \sum_{i=1}^{n} \|H_i(x,y,z)\|^{\gamma_i} = 1, \qquad (1)$$

where $H_i(x,y,z) = a_i x + b_i y + c_i z + d_i$.

At varying of parameters defining the individual components, different convex shapes can be represented (see figure 2). The requirements for having closed surfaces are that the exponents γ_i are positive, and that $\|H_i(x,y,z)\| \leq 1$ (the geometric meaning is that

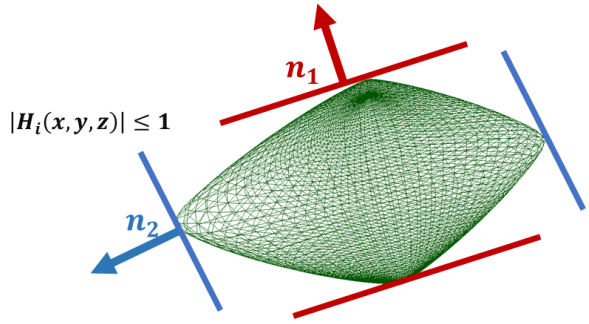

Figure 3: ***Hyperquadric definition:*** *for each component, all points of the surface are contained between the plane strip represented by equations $H_i(x,y,z) = 1$ and $H_i(x,y,z) = -1$.*

for each component, all points of the surface are contained between the plane strip represented by equations $H_i(x,y,z) = 1$ and $H_i(x,y,z) = -1$ (see figure 3).

4. Point cloud fitting

Point cloud fitting consists in finding the optimal parameterization of an hyperquadric given a set of points known to be on its boundary. In this section, we describe our approach to efficiently perform this task.

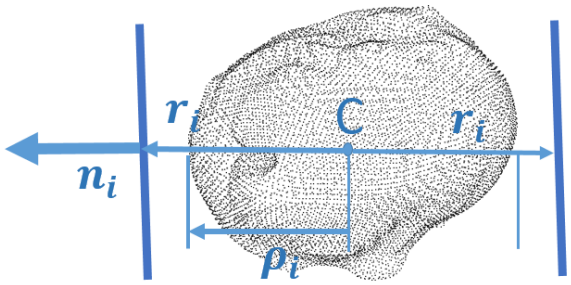

Figure 4: ***Hyperquadric parametrization:*** *the center of mass of the point cloud C is the origin of the reference system. For each patch H_i, plane strip width r_i is parametrized by applying a scale factor σ_i to the bounding distance ρ_i which is computed by projecting the point cloud with respect to the plane normal n_i.*

Parametrization. Given the equation of the hyperquadrics, each component can be parametrized with respect to the point cloud to fit. The original formulation (see Eq. 1) describes each component as a plane equation represented by coefficients (a_i, b_i, c_i, d_i), which are difficult to manage since they can vary indefinitely and they have no specific physical meaning. Hence, in order to reduce the number of parameters and to have better control of constraints, we derived a specific parametrization. We considered the center of mass of the point cloud C as origin of the reference system (see Fig. 4). Thus, the components $H_i(x,y,z)$ can be written as

$$n_{xi}x + n_{yi}y + n_{zi}z = r_i, \tag{2}$$

where $n_i = (n_{xi}, n_{yi}, n_{zi}) = (\cos\phi_i \cos\theta_i, \sin\phi_i \cos\theta_i, \sin\theta_i)$ is the unit vector representing the plane normal, and r_i is the plane distance from the center of mass. The latter can be further parametrized as $r_i = \rho_i(1+\sigma_i)$, where ρ_i is the bounding distance for the point cloud with respect to the normal n_i, and s_i is a scale factor for stretching or compressing the plane strip (see figure 4). Given that the bounding distance ρ_i can be computed for each plane with respect to the point cloud, for each patch H_i of the hyperquadrics we can control the width of the plane strip just by modifying the scale factor s_i. Finally, the exponent factor can be written as $\gamma_i = 2\varepsilon_i$, in order to remove the norm operation. In this way, each component $H_i(x,y,z)$ can be represented by four parameters:

$$\pi(H_i) = (\phi_i, \theta_i, \sigma_i, \varepsilon_i) \tag{3}$$

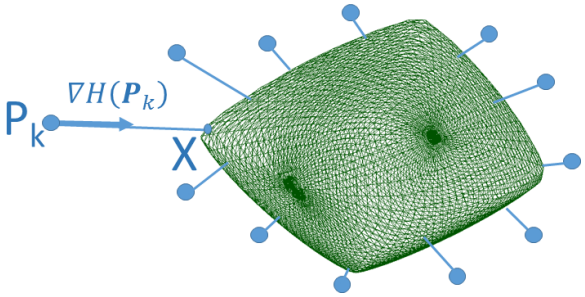

Figure 5: ***Least-square problem:*** *the optimal implicit parametrization is found by minimizing the square distance of the input points with respect to the algebraic surface. Euclidean distance is approximated by using first order Taylor expansion.*

Least-square problem. Given a point cloud $(p_1, p_2, .., p_K)$, the problem of fitting an hyperquadric surface can be expressed as a non-linear optimization problem where the target is to find the optimal parametrization $\Pi(H) = (\pi(H_1), \pi(H_2), ..., \pi(H_N))$ that minimizes the distance of the samples with respect to the surface represented by implicit function $H(x,y,z)$:

$$\Pi(H) = argmin \sum_{k=1}^{K} d^2(p_k, H), \tag{4}$$

where the distance between a given sample p_k and the surface can be computed algebraically,

$$d_a^2(p_k, H) = (H(x_k, y_k, z_k) - 1)^2, \tag{5}$$

but better accuracy can be obtained by estimating the Euclidean distance between the sample p_k and the hyperquadric surface (see figure 5). Specifically, considering the first-order Taylor expansion of the hyperquadric function, we have

$$H(x) \approx H(p_k) + \nabla H(p_k) \cdot (x - p_k), \tag{6}$$

and imposing $H(x) = 1$, we get

$$d^2(p_k, H) = \|x - p_k\|^2 \approx \frac{d_a^2(p_k, H)}{\|\nabla H(p_k)\|^2}, \tag{7}$$

that can be used for computing the cost function. To this end, we can note that the gradient operator can be computed in analytical

form from the hyperquadric definition:

$$\nabla H(x,y,z) = \sum_i \gamma_i (a_i x + b_i y + c_i z + d_i)^{\gamma_i - 1}(a_i, b_i, c_i). \quad (8)$$

For solving the constrained minimization problem, we consider the Levenberg-Marquardt method [Lou05], using as a first guess an ellipsoid approximation with the plane normals and distances computed with respect to the oriented bounding box of the input point cloud [KHGB95]. For each iteration, bounding distances of plane strips are computed with respect to the plane normals defined by parameters ϕ_i,θ_i, and the scale factors s_i are applied over it.

5. Explicit representation

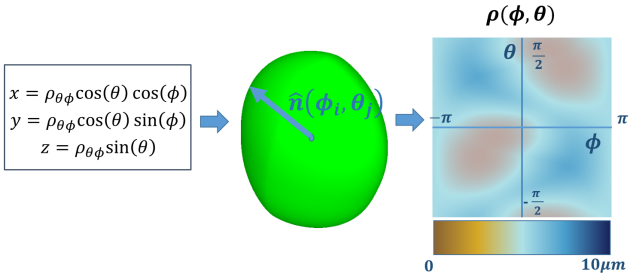

Figure 6: ***Explicit representation:*** *given the implicit representation of an hyperquadrics, the explicit representation is computed by considering spherical coordinates and computing radii on a regular sampling basis.*

While the implicit representation recovered in the previous section provides a very good shape descriptor, for a number of tasks, e.g., tessellation, it is handy to also have an equivalent explicit representation, capable to generate 3D points given a few parameters. However, given an implicit representation of an hyperquadric, there is no way to recover and explicit representation in closed form. We thus compute, through numerical optimization, a best fit spherical coordinates formulation

$$\begin{aligned} x &= \rho(\theta,\phi)\cos\theta\cos\phi \\ y &= \rho(\theta,\phi)\cos\theta\sin\phi \\ z &= \rho(\theta,\phi)\sin\theta, \end{aligned}$$

where the function $\rho(\theta,\phi)$ varies according to the angles, and needs to be computed for a given sampling of the unit sphere. In our case, we consider a regular sampling, and for each couple of angles (θ,ϕ) we solve an optimization problem with Levenberg-Marquardt to find the optimal radius ρ such that the algebraic distance from the implicit function is minimal:

$$\rho(\theta,\phi) = argmin(H(x,y,z) - 1)^2. \quad (9)$$

Fig. 6 shows a schematic representation of the optimization process and the graphic representation of the explicit parametrization of an hyperquadric implicit function. The obtained samples are used for tessellating the hyperquadrics surface, for evaluating the fitting errors, and for visual comparisons with respect to the original shape.

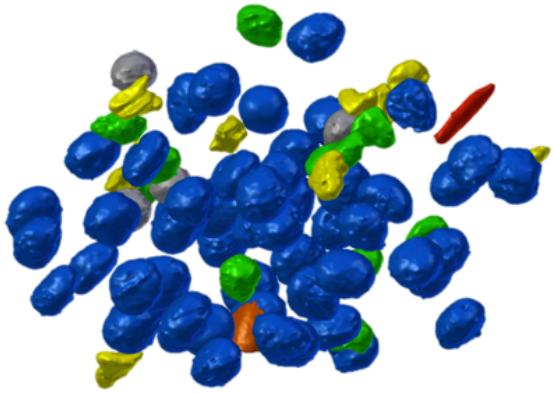

Figure 7: ***Input nuclei envelopes:*** *the analysis framework was tested on a collection of 92 3D reconstructions of brain cell nuclei extracted from a sample of layer VI somatosensory cortex of a juvenile rat (Fig. 8).*

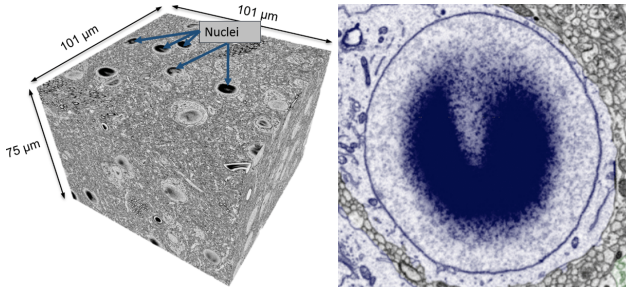

Figure 8: ***Dataset acquisition.*** *Left: dataset obtained by imaging a volume of brain parenchyma from layer VI somatosensory cortex of a P14 rat, using a serial block-face scanning electron microscopy (SBEM) with a 3View module. Right: neuronal nuclei present the dark artifact typical of electrons accumulating in portions of the sample where there is low density of biological material.*

6. Results

Our framework was implemented in C++, by adapting the levmar implementation of the Levenberg-Marquardt algorithm [Lou05]. Our test case was a collection of 92 3D reconstructions of brain cells nuclei (Fig. 7). The models were extracted from dense reconstructions obtained by semiautomatic segmentation of nanometric scale electron microscopy stacks, obtained after imaging a volume of brain parenchyma from layer VI somatosensory cortex of a P14 rat using a serial block-face scanning electron microscopy (SBEM) with a 3View module (Fig. 8 left).

Fitting analysis. Given the collection of nuclear point clouds, we evaluated the quality of fitting by considering a hyperquadrics implicit representation containing $N = 3$ patches. The fitting procedure used the following constraints for the patch parameters: $-\pi \leq \phi_i \leq \pi$, $-\frac{\pi}{2} \leq \theta_i \leq \frac{\pi}{2}$, $-0.1 \leq \sigma_i \leq 0.5$, $0.75 \leq \varepsilon_i \leq 2.5$. Table 1 shows the statistics about the nuclear envelopes which were fitted with our implicit model: specifically the number of cells for

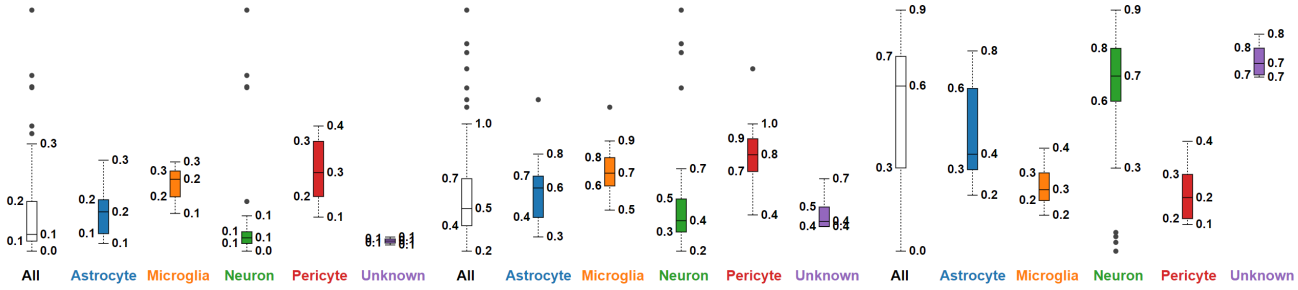

Figure 9: ***Fitting error:*** *three metrics are considered for evaluating the quality of fitting. The average distance error in µm(left), the maximum distance error in µm(center), and the percent of samples with distance error below the threshold of* $0.1\mu m$*(right).*

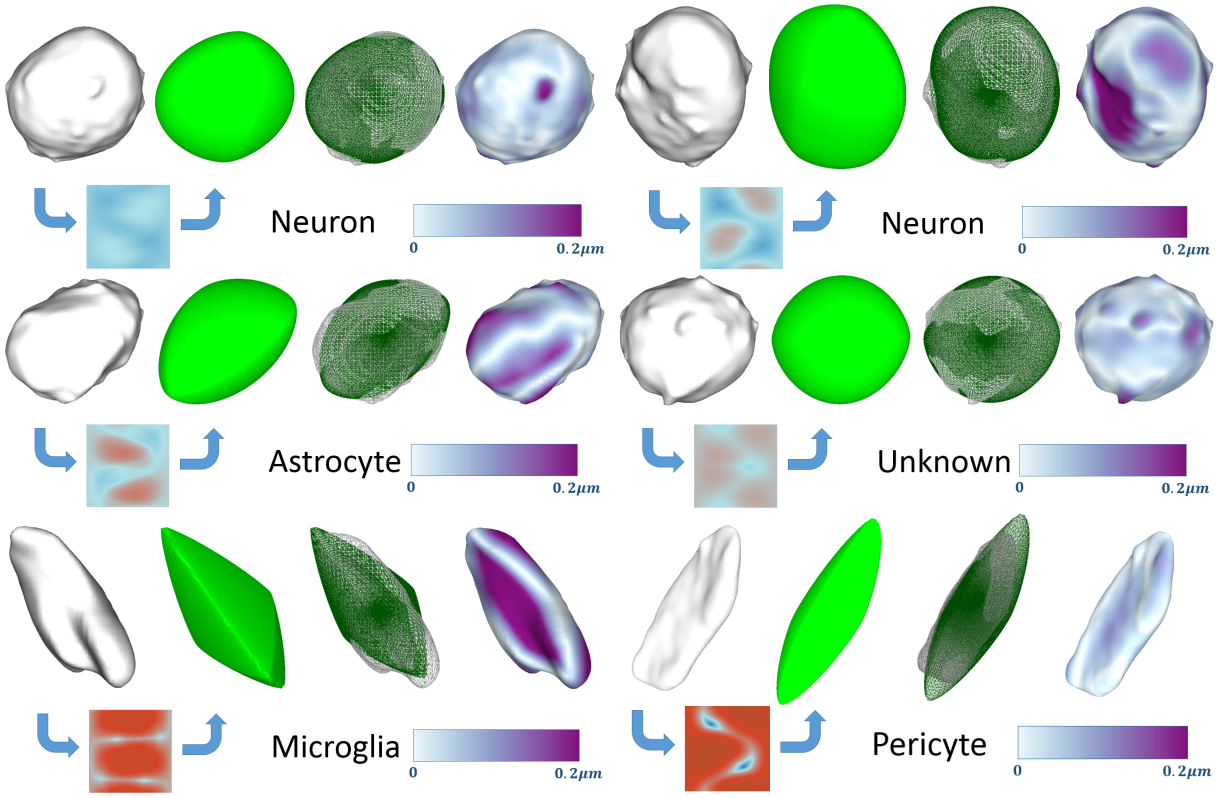

Figure 10: ***Visual assessment of cellular envelope parametrization:*** *for each nuclear shape, from left to right, the input shape, the fitting hyperquadric and the computed explicit representation, the models superimposed, and the input model color-mapped with distance error in µm. The color-map employed is the BuPu Colorbrewer scheme [HB03], and the models are rendered using MeshLab software [CCC*08].*

a given category, the average number of point samples, the average volume and the standard deviation and the average fitting time (a maximum of 1000 iteration was considered during the optimization process). All fitting sessions were performed on a laptop equipped with a CPU Intel i7-4700HQ running Linux Ubuntu Kernel version 3.13. For each nuclear envelope, we considered three evaluation metrics: the average and max distance error for the points in the shape (computed by using equation 7), and the percent of points whose distance error is below $0.1\mu m$. Fig. 9 shows boxplots of these error metrics for the various cell categories: it appears that the fitting is more accurate for neuron nuclei, while it is less accurate for shapes with concavities like microglia or pericytes. For visual reference, Fig. 10 shows some examples of fitting obtained with our model for various kind of nuclear shapes. The original input shape is shown together with the tessellated hyperquadric representation, as well as its explicit radial representation (for explicit representation we consider a regular sampling of $64x64$ on the angle domain (ϕ,θ)). Moreover, the fitting error is color mapped to the original shape, by employing the BuPu colorbrewer scheme [HB03] (color scale from 0 to 0.2 μm). From Fig. 10, it appears that our paramet-

Type	# Cells	# Avg Verts	Volume(μm^3)	Time(m)
Neurons	58	9261	715.7 ± 13.01	3.68
Astrocytes	11	9467	349.3 ± 18.88	4.28
Microglia	11	7780	185.5 ± 18.7	3.62
Pericytes	8	7224	120.1 ± 13.3	4.21
Unknown	4	10085	427 ± 24.9	4.42

Table 1: ***Nuclei statistics:*** *listing showing the number of nuclear envelopes, the average number of point samples, the volume size in μm^3 with the standard deviation, and the average processing time for finding the hyperquadric parametrization for each class of cells.*

ric model is accurate for convex shapes, like neurons, astrocytes and unknown cells (see the first two rows in figure 10), while it suffers in cases where the original shape is irregular, like microglia and pericytes (see last row in figure 10).

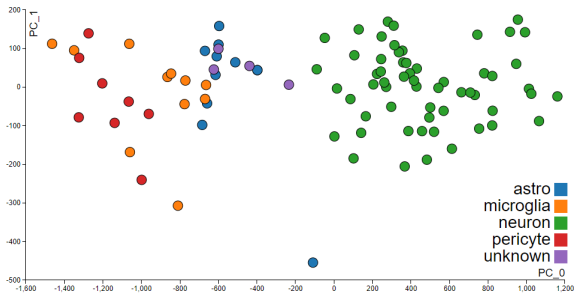

Figure 11: ***Principal component analysis:*** *the implicit parameters were reduced in order to evaluate clustering of various cell types.*

Nuclei analysis. Cells and their nuclear envelopes were first classified by domain scientists through visual assessment of morphology features. Starting from neurons, their nuclei appeared to be almost spherical, and also the largest on average compared to the other cell types. Interestingly, all neuronal nuclei presented the dark artifact typical of electrons accumulation occurring in portions of the sample where there is low density of biological material, and therefore are poorly conductive, like the lumen of the blood vessel (Fig. 8 right). On the other hand, astrocyte nuclei have an irregular shape, and are smaller than in neurons, and the microglial nuclei are smaller than neurons and appear squashed. For statistical analysis, domain scientists considered as main parameter the size of the volume. For the considered brain portion, the volume size computation showed that neurons had the biggest nuclei, followed by astrocytes and unknown cells, last two being statistically similar (Holm-Sidak's multiple comparison test; $t = 1.54$). Microglia and pericytes were similar (Holm-Sidak's comparison test, $t = 1.72$) (see numerical values in table 1). In order to improve nuclei analysis, we considered our implicit parametrization model, and we performed a preliminary Principal Component Analysis [Shl14] on the hyperquadrics parameters (namely distances r_i and exponents ε_i), as a way to automatically cluster nuclear envelopes. Fig. 11 shows the results of data reduction on hyperquadrics parametrization projected in 2D. It can be seen that our implicit model coupled with PCA efficiently discriminates particular classes of cells, while it is not reliable for recognizing other nuclear envelopes. Specifically, neurons (green) form a well-defined cluster which is clearly separated from all other classes. On the other side, two main clusters are recognizable, formed by astrocyte and unknown cells (blue and violet), and by microglia and pericytes(orange and red). These results confirm and extend the original classification by domain scientists that was based on the volume of nuclear envelopes.

7. Conclusions

We presented a framework for shape analysis of 3D nuclear envelopes of brain cells obtained from nanoscale digital reconstruction of mouse brain samples imaged with face-block scanning electron microscope. Our method is based on an implicit parametrization of 3D surface derived by adapting the classical hyperquadrics formulation [OS01]. We preliminary tested our model on a collection of 92 brain nuclear envelopes extracted from a sample of brain parenchyma from layer VI somatosensory cortex of a P14 rat. Our preliminary results show that the model can accurately represent convex neural nuclei, while the fitting performances degrade for other envelopes exhibiting concavities (specifically microglia and pericytes). We also performed a preliminary classification by employing principal component analysis, which showed that our implicit model can be considered reliable for discriminating neural nuclei shapes, but it cannot be considered accurate for discriminating other classes. To this end, in future we plan to explore the potentialities of our shape analysis framework by considering different parameterizations, like spherical harmonics [SFM09], and different data reduction techniques, like t-SNE [MH08]. We expect that more general function-based decompositions should be able to correctly represent also nuclear envelopes exhibiting concavities. Finally, we plan to extend the analysis to other 3D nuclear envelope collections characterized by different conditions.

Acknowledgments. This work was supported by the CRG grant no.2313 from King Abdullah University of Science and Technology *KAUST-EPFL Alliance for Integrative Modeling of Brain Energy Metabolism*. We also acknowledge the contribution of Sardinian Regional Authorities under project VIGEC.

References

[AK13] AVENEL C., KULIKOVA M. S.: Marked point processes with simple and complex shape objects for cell nuclei extraction from breast cancer h&e images. In *Medical Imaging 2013: Digital Pathology* (2013), vol. 8676, p. 86760Z. 2

[AM12] ALI S., MADABHUSHI A.: An integrated region-, boundary-, shape-based active contour for multiple object overlap resolution in histolog.imagery. *IEEE trans. on med. imag. 31*, 7 (2012), 1448–1460. 2

[Bar81] BARR A. H.: Superquadrics and angle-preserving transformations. *IEEE Computer graphics and Appl. 1*, 1 (1981), 11–23. 2

[CBB*16] CALÌ C., BAGHABRA J., BOGES D. J., HOLST G. R., KRESHUK A., HAMPRECHT F. A., SRINIVASAN M., LEHVÄSLAIHO H., MAGISTRETTI P. J.: Three-dimensional immersive virtual reality for studying cellular compartments in 3d models from em preparations of neural tissues. *J. of Comp. Neurology 524*, 1 (2016), 23–38. 1, 3

[CC96] COHEN I., COHEN L. D.: A hybrid hyperquadric model for 2-d and 3-d data fitting. *Computer Vision and Image Understanding 63*, 3 (1996), 527–541. 3

[CCC*08] CIGNONI P., CALLIERI M., CORSINI M., DELLEPIANE M., GANOVELLI F., RANZUGLIA G.: MeshLab: an Open-Source Mesh Processing Tool. In *Eurographics Italian Chapter Conf.* (2008), pp. 1–8. 6

[CP00] CONG G., PARVIN B.: Model-based segmentation of nuclei. *Pattern recognition 33*, 8 (2000), 1383–1393. 3

[CSS*12] CARDONA A., SAALFELD S., SCHINDELIN J., ARGANDA-CARRERAS I., PREIBISCH S., LONGAIR M., TOMANCAK P., HARTENSTEIN V., DOUGLAS R. J.: Trakem2 software for neural circuit reconstruction. *PloS one 7*, 6 (2012), e38011. 3

[DG95] DESBRUN M., GASCUEL M.-P.: Animating soft substances with implicit surfaces. In *Proc. SIGGRAPH* (1995), pp. 287–290. 2

[FHWV97] FRICKER M., HOLLINSHEAD M., WHITE N., VAUX D.: Interphase nuclei of many mammalian cell types contain deep, dynamic, tubular membrane-bound invaginations of the nuclear envelope. *The Journal of cell biology 136*, 3 (1997), 531–544. 1

[GB93] GUPTA A., BAJCSY R.: Volumetric segmentation of range images of 3d objects using superquadric models. *CVGIP: Image understanding 58*, 3 (1993), 302–326. 2

[Han88] HANSON A. J.: Hyperquadrics: smoothly deformable shapes with convex polyhedral bounds. *Computer vision, graphics, and image processing 44*, 2 (1988), 191–210. 2, 3

[HB03] HARROWER M., BREWER C. A.: Colorbrewer.org: an online tool for selecting colour schemes for maps. *The Cartographic Journal 40*, 1 (2003), 27–37. 6

[HBK*16] HOLST G., BERG S., KARE K., MAGISTRETTI P., CALI C.: Adding large em stack support. In *Information Technology (Big Data Analysis)(KACSTIT), Saudi Int. Conf. on* (2016), IEEE, pp. 1–7. 3

[HGB93] HAN S., GOLDGOF D. B., BOWYER K. W.: Using hyperquadrics for shape recovery from range data. In *Proc. ICCV* (1993), pp. 492–496. 3

[HJLC18] HÄRTEL S., JARA J., LEMUS C., CONCHA M.: 3d morphotopological analysis of asymmetric neuronal morphogenesis in developing zebrafish. *Computational modelling of objects represented in images. Fundamentals, methods and applications 6* (2018), 215–220. 3

[JKCO10] JUNG C., KIM C., CHAE S. W., OH S.: Unsupervised segmentation of overlapped nuclei using bayesian classification. *IEEE Trans. on Biomedical Engineering 57*, 12 (2010), 2825–2832. 2

[KHGB95] KUMAR S., HAN S., GOLDGOF D., BOWYER K.: On recovering hyperquadrics from range data. *IEEE Trans. on Pattern Analysis and Machine Intelligence 17*, 11 (1995), 1079–1083. 5

[KMWL08] KNOTT G., MARCHMAN H., WALL D., LICH B.: Serial section scanning electron microscopy of adult brain tissue using focused ion beam milling. *The Journal of Neurosc. 28*, 12 (2008), 2959–2964. 3

[KVRKB*15] KAYNIG V., VAZQUEZ-REINA A., KNOWLES-BARLEY S., ROBERTS M., JONES T. R., KASTHURI N., MILLER E., LICHTMAN J., PFISTER H.: Large-scale automatic reconstruction of neuronal processes from electron microscopy images. *Medical Image Analysis 22*, 1 (2015), 77 – 88. 3

[KVRR12] KULIKOVA M., VEILLARD A., ROUX L., RACOCEANU D.: Nuclei extraction from histopathological images using a marked point process approach. In *Medical Imaging 2012: Image Processing* (2012), vol. 8314, p. 831428. 2

[Lou05] LOURAKIS M. I.: A brief description of the levenberg-marquardt algorithm implemented by levmar. *Foundation of Research and Technology 4*, 1 (2005), 1–6. 5

[MH08] MAATEN L. V. D., HINTON G.: Visualizing data using t-sne. *Journal of machine learning research 9*, Nov (2008), 2579–2605. 7

[NTDS14] NG B., TOEWS M., DURRLEMAN S., SHI Y.: Shape analysis for brain structures. In *Shape Analysis in Medical Image Analysis*. Springer, 2014, pp. 3–49. 3

[OS01] OHUCHI M., SAITO T.: Three-dimensional shape modeling with extended hyperquadrics. In *3-D Digital Imaging and Modeling, 2001. Proc. Third Int. Conf. on* (2001), IEEE, pp. 262–269. 3, 7

[Pen86] PENTLAND A. P.: Perceptual organization and the representation of natural form. *Artif. Intell. 28*, 3 (May 1986), 293–331. 2

[QWBW08] QUEISSER S. G., WITTMANN M., BADING H., WITTUM G.: Filtering, reconstruction, and measurement of the geometry of nuclei from hippocampal neurons based on confocal microscopy data. *Journal of Biomedical Optics 13*, 1 (2008), 014009. 1, 3

[QXFY12] QI X., XING F., FORAN D. J., YANG L.: Robust segmentation of overlapping cells in histopathology specimens using parallel seed detection and repulsive level set. *IEEE Trans. on Biomedical Engineering 59*, 3 (2012), 754–765. 2

[RR16] RAM S., RODRIGUEZ J. J.: Size-invariant detection of cell nuclei in microscopy images. *IEEE trans. on medical imaging 35*, 7 (2016), 1753–1764. 2

[SB90] SOLINA F., BAJCSY R.: Recovery of param. models from range images: The case for superquadrics with global deform. *IEEE trans. on patt. anal. and machine intell. 12*, 2 (1990), 131–147. 2

[SFM09] SHEN L., FARID H., MCPEEK M. A.: Modeling three-dimensional morphological structures using spherical harmonics. *Evolution: International Journal of Organic Evolution 63*, 4 (2009), 1003–1016. 2, 3, 7

[Shl14] SHLENS J.: A tutorial on principal component analysis. *arXiv preprint arXiv:1404.1100* (2014). 7

[SSKH11] SOMMER C., STRAEHLE C., KÖTHE U., HAMPRECHT F. A.: Ilastik: Interactive learning and segmentation toolkit. In *2011 IEEE international symposium on biomedical imaging: From nano to macro* (2011), IEEE, pp. 230–233. 3

[SZW16] SHI J., ZHANG W., WANG Y.: Shape analysis with hyperbolic wasserstein distance. In *Proceedings of the IEEE Conference on Computer Vision and Pattern Recognition* (2016), pp. 5051–5061. 3

[TM90] TERZOPOULOS D., METAXAS D.: Dynamic 3d models with local and global deformations: Deformable superquadrics. In *Computer Vision, 1990. Proceedings, Third International Conference on* (1990), IEEE, pp. 606–615. 2

[TPG99] TREECE G. M., PRAGER R. W., GEE A. H.: Regularised marching tetrahedra: improved iso-surface extraction. *Computers & Graphics 23*, 4 (1999), 583–598. 3

[TRU98] THÉVENAZ P., RUTTIMANN U., UNSER M.: A pyramid approach to subpixel registration based on intensity. *IEEE Trans. on Image Processing 7*, 1 (January 1998), 27–41. 3

[VVDK*13] VETA M., VAN DIEST P. J., KORNEGOOR R., HUISMAN A., VIERGEVER M. A., PLUIM J. P.: Automatic nuclei segmentation in h&e stained breast cancer histopathology images. *PloS one 8*, 7 (2013), e70221. 2

[VVLVDDH13] VINK J. P., VAN LEEUWEN M., VAN DEURZEN C., DE HAAN G.: Efficient nucleus detector in histopathology images. *Journal of microscopy 249*, 2 (2013), 124–135. 2

[WGK*15] WACHINGER C., GOLLAND P., KREMEN W., FISCHL B., REUTER M., ET AL.: Brainprint: A discriminative characterization of brain morphology. *NeuroImage 109* (2015), 232–248. 3

[WHS*12] WIENERT S., HEIM D., SAEGER K., STENZINGER A., BEIL M., HUFNAGL P., DIETEL M., DENKERT C., KLAUSCHEN F.: Detection and segmentation of cell nuclei in virtual microscopy images: a minimum-model approach. *Scientific reports 2* (2012), 503. 2

[WQE*09] WITTMANN M., QUEISSER G., EDER A., WIEGERT J. S., BENGTSON C. P., HELLWIG A., WITTUM G., BADING H.: Synaptic activity induces dramatic changes in the geom. of the cell nucleus: interplay between nuclear structure, histone h3 phosphorylation, and nuclear calcium signaling. *Journ. of Neurosc. 29*, 47 (2009), 14687–14700. 1, 3

[XBC18] XIAO P., BARNES N., CAETANO T.: 3-d shape matching and non-rigid correspondence for hippocampi based on markov random fields. *IEEE Trans. on Image Processing 27*, 3 (2018), 1271–1281. 3

[XY16] XING F., YANG L.: Robust nucleus/cell detection and segmentation in digital pathology and microscopy images: a comprehensive review. *IEEE reviews in biomedical eng. 9* (2016), 234–263. 1, 2